SCIENCE CHINA
Physics, Mechanics & Astronomy

• Article •

September 2020 Vol. 63 No. 9: 297811
https://doi.org/10.1007/s11433-019-1526-3

Kondo resonance assisted thermoelectric transport through strongly correlated quantum dots

YongXi Cheng[1,2], ZhenHua Li[3], JianHua Wei[4*], HongGang Luo[3,1*], HaiQing Lin[1], and YiJing Yan[5]

[1]*Beijing Computational Science Research Center, Beijing 100193, China;*
[2]*Department of Science, Taiyuan Institute of Technology, Taiyuan 030008, China;*
[3]*School of Physical Science and Technology, Key Laboratory for Magnetism and Magnetic Materials of the MoE, Lanzhou University, Lanzhou 730000, China;*
[4]*Department of Physics, Renmin University of China, Beijing 100872, China;*
[5]*Hefei National Laboratory for Physical Sciences at the Microscale, University of Science and Technology of China, Hefei 230026, China*

Received December 18, 2019; accepted February 13, 2020; published online April 30, 2020

We theoretically studied the thermoelectric transport properties of a strongly correlated quantum dot system in the presence of the Kondo effect based on accurate numerical evaluations using the hierarchical equations of motion approach. The thermocurrent versus gate voltage shows a distinct sawtooth line-shape at high temperatures. In particular, the current changes from positive (hole charge) to negative (particle charge) in the electron number $N = 1$ region due to the Coulomb blockade effect. However, at low temperatures, where the Kondo effect occurs, the thermocurrent's charge polarity reverses, along with a significantly enhanced magnitude. As anticipated, the current sign can be analyzed by the occupation difference between particle and hole. Moreover, the characteristic turnover temperature can be further defined at which the influences of the Coulomb blockade and Kondo resonance are in an effective balance. Remarkably, the identified characteristic turnover temperature, as a function of the Coulomb interaction and dot-lead coupling, possessed a much higher value than the Kondo temperature. When a magnetic field is applied, a spin-polarized thermocurrent can be obtained, which could be tested in future experiments.

thermoelectric transport, strongly correlated quantum dot, Kondo resonance, spin-polarized thermocurrent

PACS number(s): 73.63.Kv, 72.20.Pa, 72.15.Qm

Citation: Y. X. Cheng, Z. H. Li, J. H. Wei, H. G. Luo, H. Q. Lin, and Y. J. Yan, Kondo resonance assisted thermoelectric transport through strongly correlated quantum dots, Sci. China-Phys. Mech. Astron. **63**, 297811 (2020), https://doi.org/10.1007/s11433-019-1526-3

1 Introduction

The research field of thermoelectricity is very active because of the ongoing energy resource crisis and environmental risks. A vast number of nanomaterials with various structures, such as molecular junctions [1-3], nanowires [4,5], and quantum dots (QDs) [6-8], are explored for their potential thermoelectric applications. These include heat rectification, low-temperature thermometry, and microrefrigerators [9-11].

Thermoelectric transport contains distinct information than that of bias voltage. It is also more difficult to investigate due to the residual current noise from thermal fluctuations. Most theoretical and experimental studies focus on the thermopower Seebeck effect in the Coulomb blockade (CB) regime [12-16]. In the QDs system, thermoelectric transport properties rely on incident electron energy, density of states, and temperature. In experiments, the thermoelectric transport properties of QDs are investigated through electron heating [13,17] and current heating techniques [14]. The observed thermopower, as a function of gate voltage,

*Corresponding authors (JianHua Wei, email: wjh@ruc.edu.cn; HongGang Luo, email: luohg@lzu.edu.cn)

shows sawtooth-like oscillations and sign-reversal characteristics [12, 14, 17]. Researchers use perturbation theory [18], nonequilibrium-Green-function formalism [16, 19, 20], numerical renormalization-group [21], and slave-boson representation [7, 22] methods in theoretical studies.

Unlike the CB effect, Kondo resonance is a many-body phenomenon that occurs only at low temperatures, where the spin of the localized moment is screened by the conduction electrons [23-26]. The resulting Kondo singlet state significantly affects the transport property through QDs [27, 28]. So far, theoretical research has been focused on thermopower (Seebeck coefficient) generated in strongly correlated QD systems [20, 21, 29-33]. As one of the fundamental thermoelectric physical quantities, thermopower is sensitive to the Kondo resonance scattering rate of conduction electrons [20, 21, 29, 32], gate voltages, and magnetic fields [33]. Costi and Zlatić [21] studied the spin-Kondo effect on the thermopower of a single-level QD system. In the Kondo-correlated QD system, the thermopower shows a clear deviation from the semiclassical Mott relation between thermopower and conductivity [34]. The magnitude and the sign of thermopower can be changed by tuning the gate voltages and magnetic fields, leading to an oscillatory behavior due to the Kondo effect [20, 33]. Moreover, thermopower is the applicable experimental tool for the study of the phase-sensitive Aharonov-Bohm interferometer [33, 35] and spin entropy flux [36].

Recently, the thermoelectric characterization of the Kondo resonance in QDs was experimentally investigated [6, 37]. It is anticipated that Kondo physics will play an important role in the thermoelectric functions of nanomaterials [38, 39]. Thermoelectric transport would be a sensitive tool to detect the nonequilibrium Kondo effect of strongly correlated QDs. Nevertheless, the thermoelectric properties of QDs in the Kondo regime is still an open question. The challenge for theoretical investigations is the accurate characterization of Kondo correlations. In this paper, we study the thermoelectric transport properties of a strongly correlated single QD system, with accurate evaluations and comparisons with a recent experiment by Svilans et al. [37], where the Kondo effect is important. However, the thermal conductance and thermopower as a function of temperature and gate voltage for the different Coulomb interactions have been investigated [21]. Thermopower, as a function of gate voltage, exhibits two sign changes at two temperature scales. Here, we focus on the thermocurrent through the strongly correlated QD system, which can be easily explored in experiments. It is observed that when increasing the energy level of the QD in the $N = 1$ regime, the thermocurrent changes from positive (hole charge) to negative (particle charge) at high temperatures due to the CB. However, the thermocurrent's charge polarity reverses with a significantly enhanced magnitude at low temperatures due to the Kondo resonance. In this study, we reproduce the experimental observations of Svilans et al. [37], identify the characteristic turnover temperature, T_c, and study the magnetic-field-dependent spin-polarized thermocurrent. Moreover, the thermocurrent sign is in agreement with the occupation difference between the particle and hole charge (eq. (5)).

2 Model and hierarchical equations of motion theory

The model we study is shown in Figure 1(a); the strongly correlated QD is tunneling coupled to two reservoirs via the dot-lead coupling strength Δ. The left lead is the hot bath (wine), and the right lead is the cold bath (blue). The temperature bias between the two reservoirs is $\Delta T = T_h - T_c$. The temperature of the system is defined as $T = (T_h + T_c)/2$. The total Hamiltonian for the QD system is

$$H = H_{QD} + H_{leads} + H_{coupling}. \quad (1)$$

Here, the strongly correlated QD part is described by the single-impurity Anderson model $H_{QD} = \sum_\sigma(\varepsilon_d + eV_g)\hat{a}_\sigma^\dagger\hat{a}_\sigma + Un_\sigma n_{\bar{\sigma}}$. The energy level of the QD, $\epsilon_d = \varepsilon_d + eV_g$, can be manipulated by the gate voltage. The operator, $\hat{a}_\sigma^\dagger$ ($\hat{a}_\sigma$), denotes creating (annihilating) a spin-σ electron with energy ϵ_d in the QD; U is the on-dot Coulomb interaction and $n_\sigma = \hat{a}_\sigma^\dagger\hat{a}_\sigma$ is the operator of the electron number of the QD. The Hamiltonian of the device leads is $H_{leads} = \sum_{k\mu\alpha=L,R}\epsilon_{k\alpha}\hat{d}_{k\mu\alpha}^\dagger\hat{d}_{k\mu\alpha}$ with

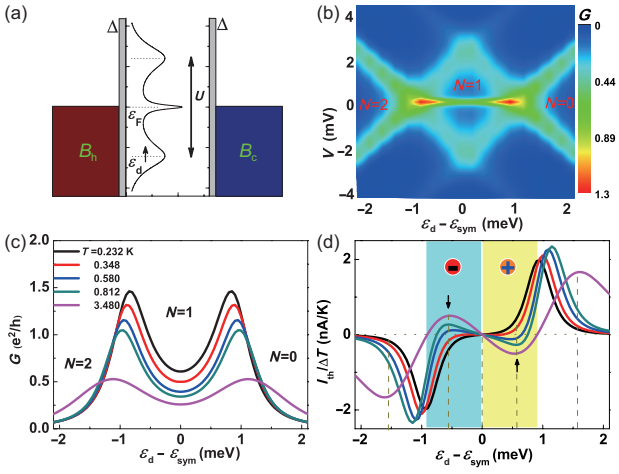

Figure 1 (Color online) (a) Schematics of thermoelectric transport through a strongly correlated single QD system. (b) The differential conductance, $G(\varepsilon_d; V)$, characterizing the charge stability of different electron numbers on the QD at a low temperature ($T = 0.348$ K). (c) The differential conductance $G(\varepsilon_d; V = 0)$, as a function of the dot energy level at different temperatures. (d) The corresponding thermocurrent, $I_{th}(\varepsilon_d; T)$. The light cyan (yellow) field indicates where the electron (hole) occupation is dominant. The parameters adopted are $W = 5.0$ meV, $\Delta = 0.2$ meV, $U = 2.2$ meV.

$\hat{d}^{\dagger}_{k\mu\alpha}(\hat{d}_{k\mu\alpha})$ corresponding to the creation (annihilation) operator of an electron with the α-reservoir state $|k\rangle$ of energy $\epsilon_{k\alpha}$. The dot-lead coupling assumes $H_{\rm coupling} = \sum_{\mu\alpha}(\hat{a}^{\dagger}_{\mu}\hat{F}^{-}_{\mu\alpha} + \hat{F}^{+}_{\mu\alpha}\hat{a}_{\mu})$, with $\hat{F}^{-}_{\mu\alpha} = \sum_k t_{k\mu\alpha}\hat{d}_{k\alpha} = (\hat{F}^{+}_{\mu\alpha})^{\dagger}$ [40]. The influence of the two leads on the interaction QD is considered through the bath spectral density function, $J_{\alpha\mu\mu'}(\omega) = \pi\sum_k t_{k\mu\alpha}t^{*}_{k\mu'\alpha}\delta(\omega - \varepsilon_{k\alpha})$ [41]. For numerical evaluations, the strongly correlated QD system is accurately solved by the hierarchical equations of motion (HEOM) formalism [40,42-44], a well-established universal and accurate method for strongly correlated systems [45-47]. The strongly correlated effect is not prominent at high temperatures. The perturbation technique of scattering can be used to solve this case. However, when the temperature is low enough, the higher-order scattering of strongly correlated interactions is so significant that the system cannot be characterized by the one-particle wave function and the perturbation technique of scattering [23]. Based on Feynman-Vernon path-integral formalism and linear response theory, HEOM theory, considering the scattering effect, can tread the strongly correlated QD system and resolve the electron-electron scattering interaction nonperturbatively for both equilibrium and nonequilibrium cases [27, 43, 48]. The HEOM formalism that governs the time evolution of dissipation density operators can be obtained as [43]:

$$\dot{\rho}^{(n)}_{j_1\cdots j_n} = -\left(\mathrm{i}\mathcal{L} + \sum_{r=1}^{n}\gamma_{j_r}\right)\rho^{(n)}_{j_1\cdots j_n} - \mathrm{i}\sum_{j}\mathcal{A}_{\bar{j}}\rho^{(n+1)}_{j_1\cdots j_n j} - \mathrm{i}\sum_{r=1}^{n}(-)^{n-r}C_{j_r}\rho^{(n-1)}_{j_1\cdots j_{r-1}j_{r+1}\cdots j_n}, \tag{2}$$

where $\mathcal{A}_{\bar{j}} \equiv \mathcal{A}^{\bar{\sigma}}_{\alpha\mu m} = \mathcal{A}^{\bar{\sigma}}_{\mu}$ and $C_{j_r} \equiv C^{\sigma}_{\alpha\mu m}$ are Grassmannian superoperators, which are illustrated in detail by Yan [40] and Jin et al. [41].

The physical quantities can be calculated using HEOM-space linear response theory. The electric current operator from bath α-lead to the system is given as:

$$\hat{I}_{\alpha} = -\frac{\mathrm{d}}{\mathrm{d}t}\left(\sum_{k}\hat{d}^{\dagger}_{k\alpha}\hat{d}_{k\alpha}\right) = -\mathrm{i}\sum_{\mu}(\hat{a}^{\dagger}_{\mu}\hat{F}^{-}_{\mu\alpha} - \hat{F}^{+}_{\mu\alpha}\hat{a}_{\mu}). \tag{3}$$

The mean current can then be evaluated in terms of dissipation density operators as $I_{\alpha}(t) = \mathrm{Tr}_{\rm T}[\hat{I}_{\alpha}\rho_{\rm T}(t)]$. The spectral function is

$$A_{\mu}(\omega) = \frac{1}{\pi}\mathrm{Re}\left\{\int_0^{\infty}\mathrm{d}t\left\{\tilde{C}_{\hat{a}^{\dagger}_{\mu}\hat{a}_{\mu}}(t) + \left[\tilde{C}_{\hat{a}_{\mu}\hat{a}^{\dagger}_{\mu}}(t)\right]^{*}\right\}\mathrm{e}^{\mathrm{i}\omega t}\right\}, \tag{4}$$

where the system correlation functions, $\tilde{C}_{\hat{a}^{\dagger}_{\mu}\hat{a}_{\mu}}(t)$ and $\tilde{C}_{\hat{a}_{\mu}\hat{a}^{\dagger}_{\mu}}(t)$, are evaluated through the time evolution of the HEOM propagator. The details of the HEOM formalism and the derivation of physical quantities are supplied by Yan [40], Jin et al. [41], and Li et al. [43].

3 Results and discussion

We present the numerical solution of the strongly correlated QD model in Figure 1(a) using the HEOM method. We assume that the parameters adopted are $U = 2.2$ meV, $W = 5.0$ meV, and $\Delta = 0.2$ meV for the on-dot Coulomb interaction, lead bandwidth, and dot-lead coupling strength, respectively. A small value was adopted for the temperature bias, $\Delta T = 0.0232$ K. For the parameters adopted above, the convergence is achieved at the truncation tier level of $L = 5$. We begin by presenting the charge stability diagram of the QD for the temperature difference, $\Delta T = 0$, and show the numerical results in Figure 1(b). Here, the temperature of the QD system is adopted as $T = 0.348$ K. The differential conductance, G, as a function of energy level, $\epsilon_{\rm d}$, and bias voltage, V, is calculated. The gate voltages can control the electron population of the QD. With the decrease in energy level, the electron numbers on the QD transform from $N = 0$ to $N = 1$ and $N = 2$. This provides the ideal platform for investigating the thermoelectric transport properties of the strongly correlated QD system considering the Kondo correlation. The differential conductance shows an increased behavior in Coulomb diamond corresponding to the odd electron numbers of the QD. The reason is that the Kondo resonance peak at the Fermi level assists electron tunneling through the QD system. To detect the thermoelectric transport properties, we present the thermocurrent over consecutive Kondo and CB regimes by altering the temperature in a wide range from $T \gg T_{\rm K}$ to $T \ll T_{\rm K}$ and show a detailed comparison with the transition of differential conductance. Figure 1(c) depicts the equilibrium differential conductance function, $G(\varepsilon_{\rm d}; V = 0)$, at different temperatures. We observe oscillations with two peaks embodied in differential conductance, G, from the energy level, -2.1 meV $< \varepsilon_{\rm d} - \varepsilon_{\rm sym} < 2.1$ meV ($\varepsilon_{\rm sym} = -U/2 = -1.1$ meV). The conductance has a minimum value at the particle-hole symmetry point. The amplitude of the conductance peaks increases with the decreasing temperature because of the enhancement of the Kondo effect. At low temperatures, the Kondo singlet state forming between the QD and conduction electrons will assist the transport process.

The thermocurrent, $I_{\rm th}$, in response to a small temperature bias ($\Delta T = 0.0232$ K), exhibits remarkably different features from its electrical-bias-induced counterpart. Figure 1(d) shows the thermocurrent through the QD system, $I_{\rm th}(\varepsilon_{\rm d}; T)$, as a function of energy level, $\varepsilon_{\rm d}$, with consecutive temperatures crossing over the Kondo and the CB regimes. At high temperatures (the CB regime, see the magenta curve with $T = 3.48$ K), the thermocurrent, $I_{\rm th}(\varepsilon_{\rm d})$, shows a distinct sawtooth shape with the energy level of the QD and oscillates around zero in the same period as the differential conductance

in Figure 1(c) [17]. The thermocurrent reveals a negative value (particle) in the $N = 2$ regime. In the $N = 1$ regime, with the increase of the energy level of the QD, the thermocurrent gives rise to a continuous transition from positive to negative values. Finally, the thermocurrent changes to a positive value (hole) in the $N = 0$ regime. Here, the thermocurrent oscillates about zero in the same period as the differential conductance in the $N = 1$ regime. The high-temperature behavior of the thermocurrent in CB agrees with previous results [13].

The most intriguing feature is the thermocurrent charge polarity reversal that occurred in the $N = 1$ domain, centered around the particle-hole symmetry point at which $I_{\rm th}(\varepsilon_{\rm d} = \varepsilon_{\rm sym}; T) = 0$. Take $I_{\rm th}(\varepsilon_{\rm d}; T = 3.48$ K) and $I_{\rm th}(\varepsilon_{\rm d}; T = 0.232$ K) as examples of the high-temperature and low-temperature cases, respectively. Both experience sign changes as $\varepsilon_{\rm d}$ crosses the symmetric point, but with reversed charge polarities. The high-temperature case (magenta curve) goes with the positive-to-negative charge polarity. The reverse charge polarity occurs in the low-temperature case (black curve). The latter also has a significantly enhanced amplitude due to the strong Kondo correlations. The above results quantitatively reproduce the experimental observations reported by Svilans et al. [37].

The physical mechanism of the observed thermocurrent characteristics can be understood as follows. In the $N = 1$ domain, the QD is an open-shell electronic structure. (i) At high temperatures, the CB effect determines the transport properties. Consequently, when the energy level is $\varepsilon_{\rm d} < \varepsilon_{\rm sym}$, the electron occupation is dominant. The CB inhibits electron hopping, whereas the hole charge is subject to strong fluctuations and becomes the dominant mechanism for the transport. So, the thermocurrent through the system exhibits a positive value when $\varepsilon_{\rm d} < \varepsilon_{\rm sym}$. On the contrary, when $\varepsilon_{\rm d} > \varepsilon_{\rm sym}$, the hole occupation becomes dominant and the CB prohibits the hole current, resulting in electron-dominant tunneling with a negative thermocurrent [34]. (ii) At low temperatures, the many-body resonant-tunneling caused by the Kondo effect is predominant. This results in a negative thermocurrent for $\varepsilon_{\rm d} < \varepsilon_{\rm sym}$ due to the underlying multi-electron-resonant tunneling. However, the Kondo singlet state will become hole-dominant when $\varepsilon_{\rm d} > \varepsilon_{\rm sym}$, leading to a positive thermocurrent through the QD. Moreover, the thermocurrent is enhanced in the Kondo regime due to the Kondo resonance peak emerging at the Fermi level, as shown in Figure 1(a) [33]. The above CB-versus-Kondo mechanism gives rise to the charge polarity reversal of the thermocurrent, $I_{\rm th}(\varepsilon_{\rm d}; T)$, as a function of $\varepsilon_{\rm d}$ in the $N = 1$ domain.

To further illustrate how the Kondo effect changes the thermoelectric transport of the strongly correlated single QD system, we also present the thermocurrent, $I_{\rm th}$, as a function of the energy level, $\varepsilon_{\rm d}$, for the different temperatures without the on-dot Coulomb interaction $U = 0$. Here, the Kondo effect is absent from the QD system. The numerical results for the thermocurrent are shown in Figure 2(a). The thermocurrent oscillations and charge polarity reversal about the energy level $\varepsilon_{\rm d} = \varepsilon_{\rm sym} = -1.1$ meV disappear. Only a simple transition from negative to positive emerges at the Fermi level, $\varepsilon_{\rm d} = 0$, due to the single-electron tunneling process. The thermal fluctuations of the QD system lead that the thermocurrent enhances remarkably with the high temperature. Hence, the novel behavior of the thermocurrent through a strongly correlated QD system manipulated by Kondo physics is different from thermoelectric transport without the Kondo effect.

As a many-body effect, the Kondo effect will lead to the spin-flip scattering of conduction electrons. So, the thermocurrent will be enhanced in the Kondo regime through the strongly correlated QD system. The on-dot Coulomb interaction of the QD system will lead the electron-electron scattering, which is very important for thermoelectric transport. We detected the thermocurrent with the different on-dot Coulomb interactions for a low temperature, $T = 0.232$ K. The numerical results are shown in Figure 2(b). We found that the single-electron tunneling peak located at $\varepsilon_{\rm d} = -U/2$ moves to the left with the increase of on-dot Coulomb interaction; the tunneling peak at the Fermi level, $\varepsilon_{\rm d} = 0$, is independent of the on-dot Coulomb interaction. In the Kondo regime, the thermocurrent is suppressed by the strong on-dot Coulomb interaction. For example, the thermocurrent at the energy level, $\varepsilon_{\rm d} - \varepsilon_{\rm sym} = -0.5$ meV, is distinct for the on-dot Coulomb interaction, $U = 2.2$ meV. By contrast, the thermocurrent becomes weak for the on-dot Coulomb interaction, $U = 2.6$ meV, and almost vanishes for the on-dot Coulomb interaction, $U = 3.0$ meV. So, the on-dot Coulomb interaction can manipulate the thermocurrent through a strongly correlated QD system in experiments.

We can identify a characteristic turnover temperature, $T_{\rm c}$, at which the influences of the CB and Kondo resonance are in an effective balance. At this temperature, the sign of the thermocurrent through the QD starts to change. To be more

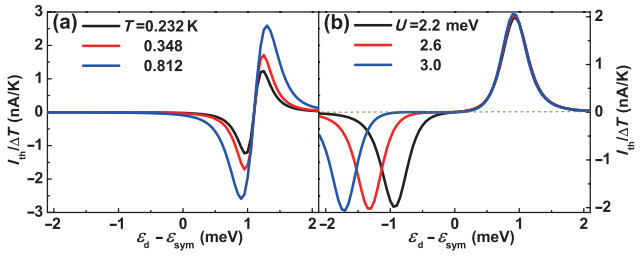

Figure 2 (Color online) (a) The thermocurrent, $I_{\rm th}$, as a function of the energy level, $\varepsilon_{\rm d}$, with the different temperatures without on-dot Coulomb interaction ($U = 0$). (b) The thermocurrent, $I_{\rm th}$, as a function of the energy level, $\varepsilon_{\rm d}$, with the different on-dot Coulomb interactions at the low temperature, $T = 0.232$ K.

specific, we focus on the particle-hole symmetry case, where $\varepsilon_d = -U/2$. The accurately evaluated T_c is reported in Figure 3. It possesses the same scaling for the different dot-lead coupling strengths, Δ, and shows a decay with the on-dot Coulomb interaction, U. For comparison, we also present the theoretical expression of Kondo temperature, $T_K = (U\Delta/2)^{1/2}\exp(-\pi U/8\Delta + \pi\Delta/2U)$. The characteristic turnover temperature, T_c, is significantly higher than the Kondo temperature, and this corresponds with the transition of the temperature scale reported by Costi and Zlatic [21]. Moreover, the characteristic turnover temperature, T_c, can also be modulated by the gate voltage. So, it provides a very useful tool for experimentally exploring the change of sign behavior in a thermocurrent.

Furthermore, the CB-versus-Kondo mechanism suggests the sign of the thermocurrent can be analyzed by the particle and hole occupancy difference,

$$\Delta N_d = \int_{-T}^{0} A(\omega)\mathrm{d}\omega - \int_{0}^{T} A(\omega)\mathrm{d}\omega, \tag{5}$$

where $A(\omega)$ denotes the equilibrium spectral function for the given QD system being studied at temperature T, in the absence of temperature bias. The sign of the thermocurrent indicates the transport carrier charge polarity, with electron (−) or hole (+) by nature, which corresponds to $\Delta N_d > 0$ and $\Delta N_d < 0$, respectively.

Figure 4 depicts the evaluated $A(\omega)$ (upper panels) and the corresponding occupancy difference ΔN_d (low panels) at $T = 3.48$ K (left panels) and $T = 0.348$ K (right panels). The two vertical dashed lines, $\omega = \pm T$, included in Figure 4(a) and (b) specify the integral frequency range relevant to ΔN_d of eq. (5). The demonstrated five values of the dot energy level correspond with those dark yellow vertical dash lines in Figure 1(d), with $\Delta\varepsilon_d \equiv \varepsilon_d - \varepsilon_{sym} = 0, \pm 0.6$ and ± 1.6 meV, where $\varepsilon_{sym} = -U/2 = -1.1$ meV. The particle-hole symmetry point $\varepsilon_d = \varepsilon_{sym}$ (color green in Figure 4), is used as a reference for the discussions below. It shows a symmetric spectral function, $A(-\omega) = A(\omega)$; thus, $\Delta N_d = 0$ (cf. eq. (5)) and $I_{th}(\varepsilon_d = \varepsilon_{sym}; T) = 0$.

It is well-known that at high temperatures, $A(\omega)$ shows only two Hubbard peaks centered around $\omega = \varepsilon_d$ and $\varepsilon_d + U$, respectively (Figure 4(a)) [23]. Both Hubbard peaks will move to the right with the increase of energy level. Meanwhile, the peak at $\omega = \varepsilon_d$ becomes high, while the peak at $\omega = \varepsilon_d + U$ becomes low. So, we have $A(\omega = \varepsilon_d) > A(\omega = \varepsilon_d + U/2)$ when $\varepsilon_d > \varepsilon_{sym}$ and vice versa. This variation of spectral function leads to ΔN_d at energy levels $\Delta\varepsilon_d \equiv \varepsilon_d - \varepsilon_{sym} = -1.6$ and 0.6 meV, being positive values. Here, the particle-like transport is dominant and associated with a negative thermocurrent. However, the ΔN_d at energy levels, $\Delta\varepsilon_d \equiv \varepsilon_d - \varepsilon_{sym} = -0.6$ and 1.6 meV, are negative values. Here, the hole-like transport is dominant and associated with the positive thermocurrent. The evaluated ΔN_d are reported in Figure 4(c), and each individual sign agrees with the charge parity of its thermocurrent counterpart, the magenta curve in Figure 1(d).

At low temperatures, the Kondo resonance singlet emerges at the Fermi level, $\omega = 0$ (Figure 4(b)). The inset highlights the resultant spectral function, $A(\omega; \Delta\varepsilon_d)$, within the relevant frequency integration window, exemplified by the pair of $\Delta\varepsilon_d = (0.6, -0.6)$ meV. The resulting Kondo peak asymmetry tilts in favor of the $\omega < 0$ domain when $\varepsilon_d < \varepsilon_{sym}$ and vice versa. The Kondo resonance singlet is electronic in nature for the energy level $\varepsilon_d < \varepsilon_{sym}$. It effectively enhances the electron transport via the level, ε_d, and reduces the hole transport in the zero-frequency domain [32]. On the contrary,

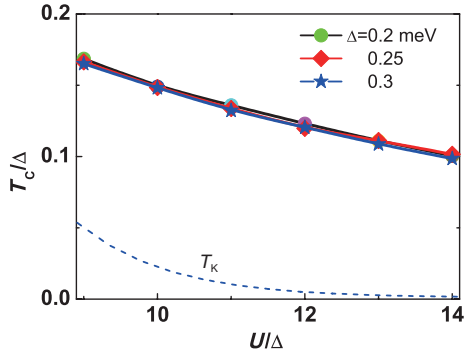

Figure 3 (Color online) The characteristic turnover temperature, T_c, as a function of the scaled on-dot Coulomb interaction. The Kondo temperature, T_K (blue dash line), is included for comparison.

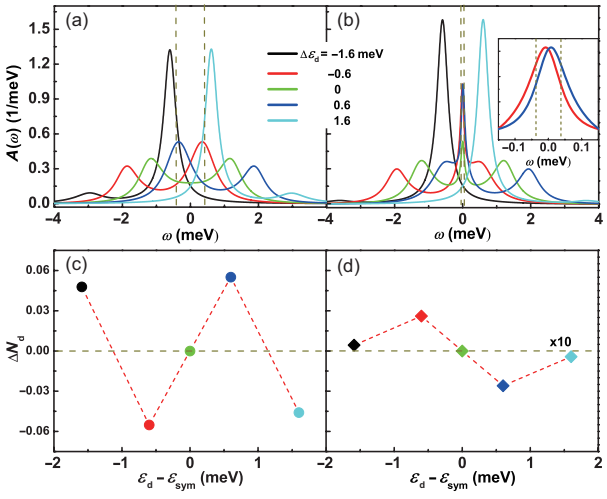

Figure 4 (Color online) The spectral function $A(\omega)$ of the QD system at (a) $T = 3.48$ K (high temperature) and (b) $T = 0.348$ K (low temperature), with the two vertical dash lines at $\omega = \pm T$. The inset of (b) highlights the asymmetrical Kondo peak of spectral function within the region of relevance to the occupancy difference, ΔN_d via eq. (5). The lower panels, (c) and (d), are the corresponding results for ΔN_d. The selected five values of ε_d for demonstration are located at the dark yellow vertical dash lines in Figure 1(d).

the Kondo resonance singlet of hole for the energy level $\varepsilon_{\rm d} > \varepsilon_{\rm sym}$ means that the hole-like transport is predominant. The corresponding evaluated values of occupancy difference, $\Delta N_{\rm d}$ eq. (5), are reported in Figure 4(d). The individual signs there all agree with the charge parity of their thermocurrent counterparts, the black curve in Figure 1(d). Moreover, charge parity reversal occurs when comparing Figure 4(d) with its high-temperature counterpart in Figure 4(c), at $\Delta\varepsilon_{\rm d} = \pm 0.6$ meV in the $N = 1$ domain.

Besides the qualitative calculation, to understand the correspondence between the spectrum function and thermoelectric transport, we can adopt the Landauer-Büttiker formula, $I_\alpha = \frac{2\pi}{h}\int {\rm d}\omega\Delta(\omega)[f_{\rm L}(\omega) - f_{\rm R}(\omega)]A(\omega)$ [43], to illustrate the transition of the thermocurrent. Here, the $f_{\rm L/R}$ is the Fermi function for the L/R-reservoir. The spectrum function that contains the Kondo physics shows a sensitive temperature dependence. This means that the spectrum function can evaluate the thermocurrent through the QD. In the Kondo regime, with the temperature decrease, the Kondo peak of the spectrum function at the Fermi level will become stronger. Here, the thermocurrent also increases with the low temperature (Figure 1(d)). Moreover, for the different dot energy level gaps, $\Delta\varepsilon_{\rm d}$, the thermocurrent can also be acquired by the Landauer-Büttiker formula.

The temperature-dependent thermoelectric transport behavior also provides an excellent trademark for exploring the Kondo effect of the strongly correlated QDs. We studied the spectral functions of the QD system for the two energy levels, $\Delta\varepsilon_{\rm d} = -0.6$ meV and $\Delta\varepsilon_{\rm d} = 0.6$ meV (marked by the black arrows in Figure 1(d)) with different temperatures in Figure 5(a) and (b), respectively. As expected, the spectral functions, $A(\omega)$, show a narrow and sharp peak at $\omega = 0$ for the low temperature. This Kondo peak of the spectral function will lead to many-body resonant-tunneling through the system. When the temperature decreases, the Kondo peak of the spectral function will become higher. The enhancement of the Kondo effect at low temperatures is consistent with the sign-reversal behavior in the thermocurrent in Figure 1(d). From the spectral functions of the QD system, we can acquire that the QD system is electron occupation for the energy level, $\Delta\varepsilon_{\rm d} = -0.6$ meV (Figure 5(a)). At low temperatures, the Kondo correlation will enhance the many-body electron-resonant tunneling, leading to a distinct negative thermocurrent associated with a larger amplitude. At the temperature, $T > T_{\rm c}$, the thermocurrent will transform into a positive value, where the Kondo effect is suppressed. Only the charge fluctuations of hole induced by the CB of a single electron dominate the transport process, with a positive thermocurrent. However, the QD system is the hole occupation at the energy level, $\Delta\varepsilon_{\rm d} = 0.6$ meV (Figure 5(b)). At low temperatures, the enhancement of the Kondo effect is the dominant mechanism for the hole-like transport, leading to a strong positive thermocurrent. When the temperature is $T > T_{\rm c}$, the hole-like transport will transform to particle-like transport because of the CB effect of the QD system. So, the thermocurrent through the QD system will have a negative value. Moreover, the positive (negative) thermocurrent is consistent with the slight slanting of the spectral function, $A(\omega)$, and the dot occupancy difference, $\Delta N_{\rm d}$, toward the left (right) for $\Delta\varepsilon_{\rm d} = -0.6$ meV (0.6 meV). Therefore, the thermocurrent that can be measured experimentally is the appropriate candidate for studying the nonequilibrium Kondo physics of the strongly correlated QD system.

To further understand the transport properties of the thermocurrent in the Kondo regime, we applied a magnetic field to the QD system and studied the temperature-dependent thermocurrent. Magnetic fields break spin degeneracy of the QD, with the energy level splitting into $\varepsilon_{\rm d} = \varepsilon_{\rm s} \pm \mu_{\rm B}B$. Moreover, the Kondo singlet resonance also splits into two much weaker branches, centered at $\omega = \pm\mu_{\rm B}B$. It provides two transport channels for the electron tunneling through the QD system. As a consequence, the spin-up and spin-down thermocurrents will separate and show different temperature dependence. This suppresses thermocurrent charge-polarity-reversal behavior due to discrimination of magnetic field against the Kondo mechanism.

Figure 6 depicts the magnetic field effects on the evaluated total thermocurrent, $I_{\rm th} = I_\uparrow + I_\downarrow$ (left panel), and the corresponding spin-polarized one, $I_{\rm sp} = I_\uparrow - I_\downarrow$ (right panel), at three representative temperatures. Both the negative thermocurrent, $I_{\rm th}$, in the $N = 2$ regime ($\varepsilon_{\rm d} - \varepsilon_{\rm sym} < -1.1$ meV) and the positive thermocurrent, $I_{\rm th}$, in the $N = 0$ regime ($\varepsilon_{\rm d} - \varepsilon_{\rm sym} > 1.1$ meV) resulting from the CB of a single electron are suppressed by the strong magnetic fields. In the $N = 1$ regime, the thermocurrent is mainly determined by the Kondo resonance at the Fermi level. Both the temperature and magnetic field destroy the Kondo effect of the QD system. The most distinctive feature is that the charge polarity reversal of the thermocurrent induced by the Kondo effect is suppressed by the temperature. Let us start with the weak magnetic field case ($\mu_{\rm B}B = 0.06$ meV), by comparing the

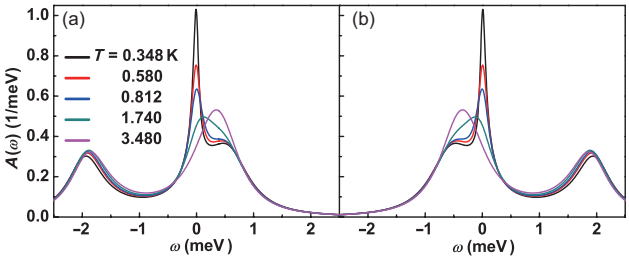

Figure 5 (Color online) The spectral function, $A(\omega)$, of the QD system with different temperatures for the energy levels, $\Delta\varepsilon_{\rm d} = -0.6$ meV (a) and $\Delta\varepsilon_{\rm d} = 0.6$ meV (b).

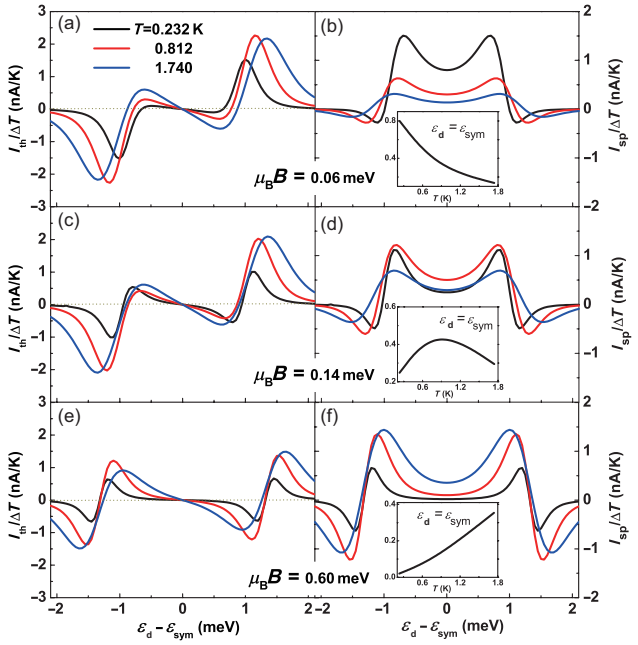

Figure 6 (Color online) The thermocurrent, $I_{\rm th}$, (left panels) as a function of the energy level, $\varepsilon_{\rm d}$, for the magnetic fields (a) $\mu_{\rm B}B = 0.06$ meV; (c) $\mu_{\rm B}B = 0.14$ meV; (e) $\mu_{\rm B}B = 0.60$ meV, at different temperatures. The right panels (b), (d), and (f) are the spin-polarized thermocurrent, $I_{\rm sp}$, for the above three magnetic fields. The insets of the right panels are the spin-polarized thermocurrents as the function of temperatures at the particle-hole symmetry point, $\varepsilon_{\rm d} = \varepsilon_{\rm sym}$.

$I_{\rm th}$ in Figure 6(a) and its spin-degenerate counterpart of Figure 1(d). Evidently, the magnetic field suppresses the Kondo correlation (at $T = 0.232$ K $< T_{\rm c}$; black curves), so it can manipulate the behavior of the thermocurrent at the low temperature. Whereas the magnetic field alters relatively little the high-temperature characteristics (at $T = 1.74$ K $> T_{\rm c}$; blue curves). When the magnetic field increases further, the thermocurrent tends to have the same variation for all temperatures. The observed sawtooth shape of $I_{\rm th}(\varepsilon_{\rm d})$ in either Figure 6(c) or (e) characterizes the CB-dominant mechanism at all temperatures in this study. Due to the characteristic turnover temperature, $T_{\rm c}$, being higher than the Kondo temperature, $T_{\rm K}$, the required magnetic field for this suppression is higher than the Kondo temperature.

Figure 6(b), (d), (f) show the spin-polarized thermocurrent with different temperatures for the three magnetic fields. The finite magnetic field will give rise to the spin-polarized thermocurrent. We found that the spin-polarized thermocurrent, $I_{\rm sp}$, in the $N = 2$ and $N = 0$ regimes shows a weak amplitude and can be enhanced by a strong magnetic field. In the $N = 1$ regime, $I_{\rm sp}(\varepsilon_{\rm sym}; T) > 0$, because $\varepsilon_{\uparrow} < \varepsilon_{\downarrow}$ and the resultant spin-specified $I_{\uparrow}$ and $I_{\downarrow}$ are dominated by hole and particle charges, respectively. For a weak magnetic field, the spin-polarized thermocurrent has a strong positive amplitude at $T < T_{\rm c}$ and decreases with the high temperature in the $N = 1$ regime (Figure 6(b)). On the contrary, the spin-polarized thermocurrent shows the contrary dependent behavior of temperature in a strong magnetic field. In the $N = 1$ regime, the spin-polarized thermocurrent is enhanced by the high temperature at a strong magnetic field (Figure 6(f)). As depicted in the insets of Figure 6, $I_{\rm sp}(\varepsilon_{\rm sym}; T)$ shows a remarkably distinct Zeeman-field dependence. As the function of temperature, it shows decreasing concave when $\mu_{\rm B}B = 0.06$ meV in Figure 6(b); non-monotonic convex when $\mu_{\rm B}B = 0.14$ meV in Figure 6(d); and increasing concave when $\mu_{\rm B}B = 0.6$ meV in Figure 6(f). The above observations arise from the interplay between the CB and Kondo effects on the spin-specified thermocurrent transport. In the weak Zeeman-field regime, the many-body resonant-tunneling induced by the Kondo effect remains dominant at low temperatures. This means that the spin-polarized thermocurrent, $I_{\rm sp}(\varepsilon_{\rm sym}; T)$, has a stronger amplitude and decreases with the temperature. For a strong Zeeman-field case, where the CB effect is dominant since the Kondo resonance is suppressed, only the thermal fluctuations of the electrons lead the weak spin-polarized thermocurrent, which increases with the high temperature. The intermediate scenario is characterized by the rich interplay between those two mechanisms. The coexistence of CB and Kondo resonance leads to the non-monotonic transition of the spin-polarized thermocurrent in the $N = 1$ regime (Figure 6(d)). It provides the most subtle and precise methods to manipulate the spin polarization transport of the strongly correlated QDs.

Finally, we present the corresponding spin-up and spin-down thermocurrent with different temperatures for the above three magnetic fields in Figure 7. It is found that the spin-specified thermocurrents, $I_{\downarrow}(\varepsilon_{\rm d} - \varepsilon_{\rm sym}; T)$ and $I_{\uparrow}(\varepsilon_{\rm d} - \varepsilon_{\rm sym}; T)$, show different magnetic field dependence.

For the energy level, $\varepsilon_{\rm d} < \varepsilon_{\rm sym}$ ($\varepsilon_{\rm sym} = -U/2 = -1.1$ meV; marked by the dark yellow short dashed line), the spin-up thermocurrent through the system has a positive value and decreases with the temperature for low magnetic fields (such as $\mu_{\rm B}B = 0.06$ meV) (Figure 7(a)). However, the spin-down thermocurrent at low temperatures has a strong negative value and is suppressed by the temperature. At temperature $T > T_{\rm c}$, the spin-down thermocurrent will change drastically into a positive value (Figure 7(b)). So, the total thermocurrent is negative, associated with the particle-like transport at low temperatures. With increasing temperatures, the total thermocurrent finally becomes positive, corresponding with the hole-like transport (Figure 6(a)). With the increase in the magnetic field, both the amplitude of the positive spin-up thermocurrent and the negative spin-down thermocurrent are suppressed (Figure 7(c) and (d)). So, a change of sign in the thermocurrent will arise with a strong magnetic field, due to the attenuation of the Kondo effect.

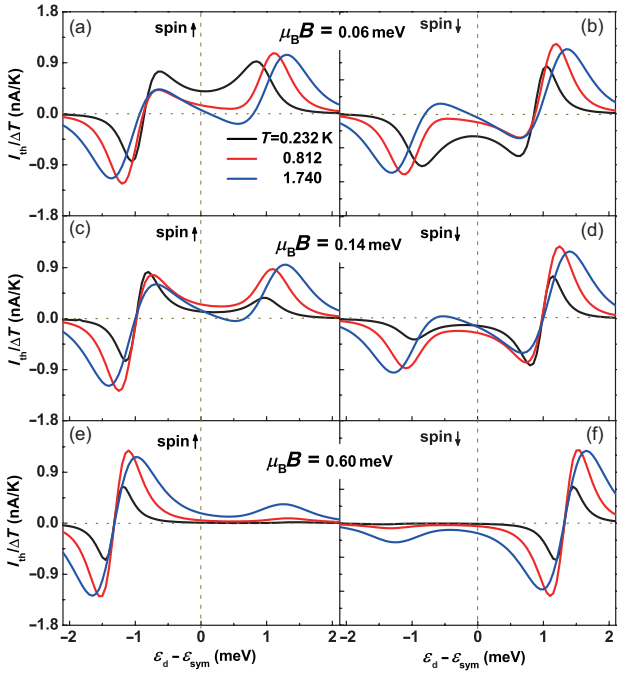

Figure 7 (Color online) The thermocurrent, $I_{\rm th}$, for spin up (left panels) and for spin down (right panels) as a function of the energy level, $\varepsilon_{\rm d}$, with different temperatures for the magnetic fields, $\mu_{\rm B}B$ = 0.06 meV ((a) and (b)), $\mu_{\rm B}B$ = 0.14 meV ((c) and (d)), and $\mu_{\rm B}B$ = 0.60 meV ((e) and (f)).

For the energy level, $\varepsilon_{\rm d} > \varepsilon_{\rm sym}$, the spin-up thermocurrent through the system at a low temperature has a positive value and is stronger than the negative spin-down thermocurrent (Figure 7(a) and (b)). So, the thermocurrent at a low temperature keeps a positive value, implying hole-like transport. Both the spin-up and spin-down thermocurrent are suppressed by the high temperature associated with the weak Kondo correlation. Finally, both the spin-up and spin-down thermocurrent have a negative value, and here particle-like transport is predominant in the QD system. So, the low-temperature transport property of a thermocurrent correlated with the Kondo effect is modulated by the magnetic field. However, the positive spin-up thermocurrent and negative spin-down thermocurrent increase with the temperature at a strong magnetic field (Figure 7(e) and (f)). Here, the Kondo effect has been suppressed. Only the thermal fluctuations of the electrons assist the transport process. Leading that the thermocurrent through the QD system is enhanced with high temperatures. As a consequence, the thermoelectric transport property of the weak magnetic field is different to those in a strong magnetic field.

4 Conclusions

In conclusion, we have studied the thermoelectric transport of a strongly correlated QD with the Kondo correlation. The thermocurrent shows a distinct sawtooth shape and gives rise to a sign reversal from a positive to a negative value at high temperatures. At low temperatures, the thermocurrent can be enhanced by the Kondo correlations, and a charge polarity reversal arises in the $N = 1$ regime. The transition behavior can be understood via the particle-versus-hole charge transport processes and the interplay between the CB and Kondo resonance. The characteristic turnover temperature at which the CB and Kondo resonance are in an effective balance is much larger than the Kondo temperature. Moreover, the magnetic-field-dependent charge polarity reversal and spin-polarized thermocurrent were also investigated. These are experimentally measurable and observable quantities for exploiting various Kondo effects that are out of equilibrium in the strongly correlated QDs.

This work was supported by the National Natural Science Foundation of China (Grant Nos. 11804245, 11747098, 11504017, 11774418, 11674139, 11834005, 21633006, and U1930402). YongXi Cheng was also supported by the China Postdoctoral Science Foundation (Grant No. 2019M660431), and the Program for the Innovative Talents of Taiyuan Institute of Technology.

1 Y. Dubi, and M. Di Ventra, Rev. Mod. Phys. **83**, 131 (2011).
2 A. Tan, S. Sadat, and P. Reddy, Appl. Phys. Lett. **96**, 013110 (2010).
3 B. C. Hsu, Y. S. Liu, S. H. Lin, and Y. C. Chen, Phys. Rev. B **83**, 041404 (2011), arXiv: 1009.5779.
4 F. Domínguez-Adame, M. Martín-González, D. Sánchez, and A. Cantarero, Physica E **113**, 213 (2019), arXiv: 1901.03046.
5 S. I. Erlingsson, A. Manolescu, G. A. Nemnes, J. H. Bardarson, and D. Sanchez, Phys. Rev. Lett. **119**, 036804 (2017).
6 B. Dutta, D. Majidi, A. García Corral, P. A. Erdman, S. Florens, T. A. Costi, H. Courtois, and C. B. Winkelmann, Nano Lett. **19**, 506 (2019), arXiv: 1811.04219.
7 M. A. Sierra, R. López, and J. S. Lim, Phys. Rev. Lett. **121**, 096801 (2018), arXiv: 1806.10505.
8 S. F. Svensson, E. A. Hoffmann, N. Nakpathomkun, P. M. Wu, H. Q. Xu, H. A. Nilsson, D. Sánchez, V. Kashcheyevs, and H. Linke, New J. Phys. **15**, 105011 (2013), arXiv: 1307.0617.
9 F. Giazotto, T. T. Heikkilä, A. Luukanen, A. M. Savin, and J. P. Pekola, Rev. Mod. Phys. **78**, 217 (2006), arXiv: cond-mat/0508093.
10 H. L. Edwards, Q. Niu, and A. L. de Lozanne, Appl. Phys. Lett. **63**, 1815 (1993).
11 M. Nahum, T. M. Eiles, and J. M. Martinis, Appl. Phys. Lett. **65**, 3123 (1994).
12 C. W. J. Beenakker, and A. A. M. Staring, Phys. Rev. B **46**, 9667 (1992).
13 A. S. Dzurak, C. G. Smith, M. Pepper, D. A. Ritchie, J. E. F. Frost, G. A. C. Jones, and D. G. Hasko, Solid State Commun. **87**, 1145 (1993).
14 A. A. M. Staring, L. W. Molenkamp, B. W. Alphenaar, H. Houten, O. J. A. Buyk, M. A. A. Mabesoone, C. W. J. Beenakker, and C. T. Foxon, Europhys. Lett. **22**, 57 (1993).
15 A. V. Andreev, and K. A. Matveev, Phys. Rev. Lett. **86**, 280 (2001), arXiv: cond-mat/0002461.
16 M. A. Sierra, and D. Sánchez, Phys. Rev. B **90**, 115313 (2014), arXiv: 1408.0181.
17 R. Scheibner, E. G. Novik, T. Borzenko, M. König, D. Reuter, A. D. Wieck, H. Buhmann, and L. W. Molenkamp, Phys. Rev. B **75**, 041301

(2007), arXiv: cond-mat/0608193.
18 D. Boese, and R. Fazio, Europhys. Lett. **56**, 576 (2001), arXiv: cond-mat/0105217.
19 M. B. Tagani, and H. R. Soleimani, Int. J. Thermophys. **35**, 136 (2014), arXiv: 1206.2007.
20 B. Dong, and X. L. Lei, J. Phys.-Condens. Matter **14**, 11747 (2002), arXiv: cond-mat/0207251.
21 T. A. Costi, and V. Zlatić, Phys. Rev. B **81**, 235127 (2010), arXiv: 1004.1519.
22 M. A. Sierra, and D. Sánchez, J. Phys.-Conf. Ser. **969**, 012144 (2018), arXiv: 1710.01069.
23 A. C. Hewson, *The Kondo Problem to Heavy Fermions* (Cambridge University Press, Cambridge, 1993).
24 J. Kondo, Prog. Theor. Phys. **32**, 37 (1964).
25 Y. Meir, N. S. Wingreen, and P. A. Lee, Phys. Rev. Lett. **70**, 2601 (1993), arXiv: cond-mat/9212007.
26 T. K. Ng, Phys. Rev. Lett. **76**, 487 (1996).
27 Y. X. Cheng, W. J. Hou, Y. D. Wang, Z. H. Li, J. H. Wei, and Y. J. Yan, New J. Phys. **17**, 033009 (2015), arXiv: 1410.1235.
28 A. E. Antipov, Q. Dong, and E. Gull, Phys. Rev. Lett. **116**, 036801 (2016), arXiv: 1508.06633.
29 T. S. Kim, and D. L. Cox, Phys. Rev. Lett. **75**, 1622 (1995), arXiv: cond-mat/9412024.
30 D. P. Daroca, P. Roura-Bas, and A. A. Aligia, Phys. Rev. B **97**, 165433 (2018), arXiv: 1804.06694.
31 J. Azema, A. M. Daré, S. Schäfer, and P. Lombardo, Phys. Rev. B **86**, 075303 (2012), arXiv: 1204.5360.
32 L. Z. Ye, D. Hou, R. Wang, D. Cao, X. Zheng, and Y. J. Yan, Phys. Rev. B **90**, 165116 (2014), arXiv: 1306.4946.
33 T. S. Kim, and S. Hershfield, Phys. Rev. Lett. **88**, 136601 (2002), arXiv: cond-mat/0110261.
34 R. Scheibner, H. Buhmann, D. Reuter, M. N. Kiselev, and L. W. Molenkamp, Phys. Rev. Lett. **95**, 176602 (2005), arXiv: cond-mat/0410671.
35 T. S. Kim, and S. Hershfield, Phys. Rev. B **67**, 165313 (2003), arXiv: cond-mat/0211554.
36 Y. Wang, N. S. Rogado, R. J. Cava, and N. P. Ong, Nature **423**, 425 (2003), arXiv: cond-mat/0406125.
37 A. Svilans, M. Josefsson, A. M. Burke, S. Fahlvik, C. Thelander, H. Linke, and M. Leijnse, Phys. Rev. Lett. **121**, 206801 (2018), arXiv: 1807.07807.
38 A. Dorda, M. Ganahl, S. Andergassen, W. von der Linden, and E. Arrigoni, Phys. Rev. B **94**, 245125 (2016), arXiv: 1608.05714.
39 D. B. Karki, and M. N. Kiselev, Phys. Rev. B **96**, 121403 (2017), arXiv: 1703.05525.
40 Y. J. Yan, J. Chem. Phys. **140**, 054105 (2014).
41 J. Jin, S. Wang, X. Zheng, and Y. J. Yan, J. Chem. Phys. **142**, 234108 (2015).
42 J. Jin, X. Zheng, and Y. J. Yan, J. Chem. Phys. **128**, 234703 (2008), arXiv: 0710.5367.
43 Z. H. Li, N. H. Tong, X. Zheng, D. Hou, J. H. Wei, J. Hu, and Y. J. Yan, Phys. Rev. Lett. **109**, 266403 (2012), arXiv: 1207.6359.
44 L. Z. Ye, X. Wang, D. Hou, R. X. Xu, X. Zheng, and Y. J. Yan, WIREs Comput. Mol. Sci. **6**, 608 (2016).
45 R. Härtle, G. Cohen, D. R. Reichman, and A. J. Millis, Phys. Rev. B **92**, 085430 (2015), arXiv: 1505.01283.
46 A. Erpenbeck, C. Hertlein, C. Schinabeck, and M. Thoss, J. Chem. Phys. **149**, 064106 (2018), arXiv: 1805.10161.
47 Z. H. Li, Y. X. Cheng, J. H. Wei, X. Zheng, and Y. J. Yan, Phys. Rev. B **98**, 115133 (2018).
48 Y. X. Cheng, Y. D. Wang, J. H. Wei, Z. G. Zhu, and Y. J. Yan, Phys. Rev. B **95**, 155417 (2017), arXiv: 1701.06369.